Ultrasound in Med. & Biol., Vol. 42, No. 2, pp. 365–377, 2016

0301-5629/$ - see front matter

http://dx.doi.org/10.1016/j.ultrasmedbio.2015.09.023

● *Original Contribution*

ULTRASOUND-BASED CAROTID ELASTOGRAPHY FOR DETECTION OF VULNERABLE ATHEROSCLEROTIC PLAQUES VALIDATED BY MAGNETIC RESONANCE IMAGING

Chengwu Huang,*† Xiaochang Pan,*† Qiong He,*† Manwei Huang,‡ Lingyun Huang,§ Xihai Zhao,*† Chun Yuan,*†¶ Jing Bai,* and Jianwen Luo*†

*Department of Biomedical Engineering, School of Medicine, Tsinghua University, Beijing, China; †Center for Biomedical Imaging Research, Tsinghua University, Beijing, China; ‡Department of Sonography, China Meitan General Hospital, Beijing, China; §Clinical Sites Research Program, Philips Research China, Shanghai, China; and ¶Department of Radiology, University of Washington, Seattle, Washington, USA

(*Received* 18 *July* 2015; *revised* 27 *August* 2015; *in final form* 23 *September* 2015)

Abstract—Ultrasound-based carotid elastography has been developed to estimate the mechanical properties of atherosclerotic plaques. The objective of this study was to evaluate the *in vivo* capability of carotid elastography in vulnerable plaque detection using high-resolution magnetic resonance imaging as reference. Ultrasound radio-frequency data of 46 carotid plaques from 29 patients (74 ± 5 y old) were acquired and inter-frame axial strain was estimated with an optical flow method. The maximum value of absolute strain rate for each plaque was derived as an indicator for plaque classification. Magnetic resonance imaging of carotid arteries was performed on the same patients to classify the plaques into stable and vulnerable groups for carotid elastography validation. The maximum value of absolute strain rate was found to be significantly higher in vulnerable plaques (2.15 ± 0.79 s^{-1}, n = 27) than in stable plaques (1.21 ± 0.37 s^{-1}, n = 19) ($p < 0.0001$). Receiver operating characteristic curve analysis was performed, and the area under the curve was 0.848. Therefore, the *in vivo* capability of carotid elastography to detect vulnerable plaques, validated by magnetic resonance imaging, was proven, revealing the potential of carotid elastography as an important tool in atherosclerosis assessment and stroke prevention. (E-mail: xihaizhao@tsinghua.edu.cn and luo_jianwen@tsinghua.edu.cn) © **2016 World Federation for Ultrasound in Medicine & Biology.**

Key Words: **Carotid atherosclerotic plaque, Elastography, Plaque classification, Rupture risk, Vulnerability.**

INTRODUCTION

Stroke is the second leading cause of death worldwide, the third leading cause of mortality in developed countries (behind only heart diseases and cancers) and the number one killer in China (National Center for Cardiovascular Diseases, China 2013; World Health Organization 2012). Rupture of carotid atherosclerotic plaques is one of the major causes of stroke (Mendel et al. 2002); thus, assessment of rupture risk (*i.e.*, vulnerability) is important to prevent the occurrence of ischemic events. Currently, evaluation of atherosclerosis typically relies on assessment of the size of plaques and the degree of stenosis (*i.e.*, narrowing of arterial lumens) using duplex ultrasound (Golemati et al. 2013; Grant et al. 2003). In clinical practice, asymptomatic patients with stenosis >70% are considered eligible for invasive revascularization procedures, such as endarterectomy and stenting (Golemati et al. 2013; Streifler 2011). However, previous studies have indicated that a substantial number of cerebrovascular events occur in arteries with less severe (<50%) stenosis (Dong et al. 2010; Saam et al. 2008; Zhao et al. 2011). In addition, it has been reported that a majority of carotid revascularization procedures in asymptomatic patients are unnecessary (Naylor 2012). Histologically, features of vulnerable plaques usually consist of a large lipid-rich necrotic core (LRNC) with thin fibrous cap, intra-plaque hemorrhage (IPH), inflammation and neovascularization (Falk et al. 1995; Finn et al. 2010). In contrast, calcification (CA) and intact surface

Address correspondence to: Xihai Zhao, Department of Biomedical Engineering, School of Medicine, Tsinghua University, Beijing 100084, China. E-mail: xihaizhao@tsinghua.edu.cn and Jianwen Luo, Department of Biomedical Engineering, School of Medicine, Tsinghua University, Beijing 100084, China. E-mail: luo_jianwen@tsinghua.edu.cn

are usually considered to be stable features. Therefore, the composition of plaques, in addition to stenosis measurements, is a critical determinant of patient risk. For these reasons, evaluation of compositional features is desirable to assess plaque rupture risk, improve diagnosis and reduce unnecessary operations.

Among the several imaging modalities used in attempts to characterize atherosclerotic plaques, magnetic resonance imaging (MRI) has been found to be the most reliable. MRI can accurately characterize almost all features of vulnerable plaques, including plaque burden (size), composition, surface condition, inflammation and neovascularization, and has been validated by histology with carotid endarterectomy specimens (Cai et al. 2002; Saam et al. 2005; Yuan et al. 2001). Good reproducibility of MRI in carotid plaque characterization has also been documented in multicenter studies and in different types of scanners, allowing wide application of MRI in studies associated with cardiovascular events and treatment monitoring (Chu et al. 2005; Phan et al. 2007; Saam et al. 2007; Underhill et al. 2008; Zhao et al. 2007). Despite its excellent performance, MRI is costly and requires long examination times. In this respect, ultrasound imaging is fast, relatively cheap and widely available and, thus, is more suitable for screening, monitoring and follow-up in large populations. In the past decade, significant emphasis has been placed on the application of ultrasound elastography (or elasticity imaging) to characterize the mechanical properties and composition of plaques. Elastography, or strain imaging, has been used to map the tissue deformation in response to an internal or external force. Because softer tissues are associated with larger deformation under the same force, elastography was first introduced to detect the pathologic variations in tissue elasticity caused by some diseases such as cancers (Ophir et al. 2000). Later, elastography was adapted for intravascular ultrasound (IVUS) to differentiate between stable and vulnerable atherosclerotic plaques in coronary arteries (de Korte et al. 1997, 2011; Shapo et al. 1996). Different strain values were found for fibrous, fatty and fibrofatty plaques, and IVUS elastography was reported to detect vulnerable plaques with high sensitivity and specificity (de Korte et al. 2000; Schaar et al. 2001). Despite these convincing results, IVUS is used predominantly for coronary arteries, rather than carotid arteries, and the main disadvantages remain its invasive nature and high cost, which limit application for screening purposes (de Korte et al. 2011).

Given the limitations of IVUS, non-invasive vascular elastography would be preferable and has been investigated by several research groups with respect to characterization of plaques in superficial arteries, mainly carotid arteries (referred to as carotid elastography) (Hansen et al. 2009; Hasegawa and Kanai 2008; Kanai et al. 2003; Korukonda and Doyley 2012; Maurice et al. 2004; Ribbers et al. 2007; Shi et al. 2008; Widman et al. 2015). In these methods, ultrasound images are non-invasively acquired either from longitudinal or transverse cross sections of the arteries at different intraluminal blood pressures. The displacement and strain distribution of the atherosclerotic plaques are estimated either on radiofrequency (RF) or B-mode data using block matching techniques such as the cross-correlation method (Ribbers et al. 2007), non-rigid image registration techniques (Richards and Doyley 2013) or optical flow-based techniques (Wan et al. 2014). Several studies have confirmed the *in vitro* and *in vivo* feasibility of carotid elastography in longitudinal views of arteries, and higher local strain was reported to be associated with softer regions, which was in good agreement with the findings from IVUS elastography (Bonnefous et al. 1996; Hasegawa and Kanai 2008; Kanai et al. 2003). Further developments necessitate carotid elastography in transverse views of the arteries in which the strain in the lateral direction (perpendicular to the ultrasound beams) is required for reconstruction of the radial strain of vessel (de Korte et al. 2011). The spatial angular compounding method was proposed to circumvent the less reliable lateral displacement estimation by reconstructing radial motion of the artery using only axial displacements acquired from multiple steering angles (Hansen et al. 2009, 2010a, 2010b; Korukonda and Doyley 2012; Korukonda et al. 2013; Nakagawa et al. 2004; Ribbers et al. 2007). More accurate 2-D displacement and strain estimation in transverse imaging planes of vessel wall have been observed with the spatial angular compounding technique, whereas further investigation is required to optimize the measurement performance (Hansen et al. 2014; Poree et al. 2015). Notably, other emerging techniques, such as acoustic radiation force impulse (ARFI) imaging, shear wave elastography (SWE), pulse wave imaging (PWI) and thermal strain imaging (TSI), have also been developed for plaque characterization (Apostolakis et al. 2015; Czernuszewicz et al. 2015; Doherty et al. 2015; Kim et al. 2008; Li et al. 2014; Widman et al. 2015). Because the present study focuses on non-invasive carotid elastography, these techniques are not discussed in detail here.

The number of studies on carotid elastography is rapidly growing, and the performance of vessel strain estimation is continuously being improved; however, validation of the techniques with *in vivo* "ground truth" is still limited. Simulation and phantom studies have been extensively performed for validation of the vascular elastography (Hansen et al. 2014; Korukonda and Doyley 2012; Maurice et al. 2004; Ribbers et al. 2007). These have the advantage of known strain or material properties. Their disadvantage may be the superoptimal image

contrast and the overly simple models of vessels or plaques, which may deviate from realistic cases. Some studies have compared vessel strain images with histologic data or mechanical testing results, which provide the morphology or mechanical properties of plaques *in vitro* as a reference (Kanai et al. 2003; Lopata et al. 2014). Sonomicrometry allows preliminary *in vitro* or *in vivo* validation by implanting crystals onto the vessel wall for motion tracking, but only enables relatively global estimation of vessel displacement and strain (Larsson et al. 2015; Widman et al. 2015). As mentioned previously, MRI has excellent *in vivo* performance for identifying different compositions of the plaques and differentiating between stable and vulnerable plaques, but very few studies have compared vascular elastography with MRI (Huang et al. 2014; Luo et al. 2013; Naim et al. 2013; Pan et al. 2014b).

The aim of this study was to quantitatively evaluate the *in vivo* capability of carotid elastography in plaque classification in patients with carotid stenosis. Under the hypothesis that high-risk features such as IPH and LRNC are softer than the stable compositions such as CA and fibrous tissue, vulnerable plaques are expected to have higher strains than stable plaques. Therefore, the maximum value of absolute strain rate (MASR), an indicator of the maximum deformation rate within the plaques, was used as a simple parameter in this study to discriminate between stable and vulnerable plaques, and the results are validated using MRI.

METHODS

Experimental protocol

This study was approved by the institutional review board of the Second Affiliated Hospital of Tsinghua University, and written informed consent was obtained from each patient. The study enrolled 197 patients between the ages of 58 and 86. Patients who had major cardiovascular events, including heart attack, stroke, myocardial infarction and transient ischemic attack, 6 mo before the examination were excluded from the study. Ultrasound scanning was performed on both the left and right carotid arteries of each patient in the supine position, and the degree of stenosis, length, thickness and area of the plaque were measured by duplex ultrasound. Afterward, sequence of ultrasound RF data were acquired mainly from the longitudinal imaging views of the plaques and stored for further strain rate imaging. Duration of acquisition was about 3–5 s to include several cardiac cycles, during which patients were asked to hold their breath. Both carotid ultrasound examinations and RF data acquisitions were conducted by a clinician with 25 y of experience using a Philips iU22 ultrasound system (Philips Medical System, Bothell, WA, USA) and an L9-3 linear array transducer. The acquired RF data were sampled at 32 MHz, and the frame rate ranged from 54 to 167 Hz, depending on the imaging depth and width. Brachial cuff blood pressures were also recorded for each patient. The same patients underwent double-blinded magnetic resonance (MR) scans for carotid arteries on a Philips Achieva TX 3.0-T MR scanner (Philips Medical System, Best, Netherlands) with a custom-designed 36-channel neurovascular coil. The imaging protocol included three multicontrast 3-D black-blood sequences with T1, T2 and heavy T1 weightings, that is, 3-D motion sensitized driven equilibrium prepared rapid gradient echo (3-D-MERGE), T2-weighted volumetric isotropic turbo spin echo acquisition (VISTA), and simultaneous non-contrast angiography and intra-plaque hemorrhage (SNAP) (Balu et al. 2011; Fan et al. 2010; Wang et al. 2013; Zhou et al. 2015). MR images were acquired in the transverse plane and covered the whole carotid artery including the common carotid artery (CCA), bifurcation (BF), internal carotid artery (ICA) and external carotid artery (ECA). Detailed parameters for the MRI protocol are listed in Table 1. The total MRI examination time for each patient was about 40 min. Patients with a maximum plaque thickness > 2.5 mm on either side were selected for strain estimation, and ultrasound signal processing and statistical analysis were performed in MATLAB R2012b (The MathWorks, Natick, MA, USA).

Ultrasound carotid elastography

Ultrasound carotid elastography was performed to estimate the strain distribution, revealing the local deformation of the plaque induced by the natural intraluminal blood pressure. Figure 1 is a schematic overview of the processing procedure. Inter-frame 2-D displacements (*i.e.*, axial and lateral displacements) and strain tensors (including axial and lateral strains and axial and lateral shear strains) were first estimated from consecutive RF frames based on a two-step optical

Table 1. MRI parameters for 3-D multicontrast sequences

	3-D-MERGE	VISTA	SNAP
Magnetic resonance sequence	TFE	TSE	TFE
TR/TE (ms)	9.3/4.3	2500/280	9.9/4.8
TFE/TSE factor	90	133	98
Field of view (mm^3)	$250 \times 250 \times 45$		
Spatial resolution (mm^3)	$0.8 \times 0.8 \times 0.8$		
Number of slices	112	112	100

3-D MERGE = 3-D motion sensitized driven equilibrium prepared rapid gradient echo; VISTA = volumetric isotropic turbo spin echo acquisition; SNAP = simultaneous non-contrast angiography and intra-plaque hemorrhage; TFE = turbo field echo; TSE = turbo spin echo; TR = repetition time; TE = echo time.

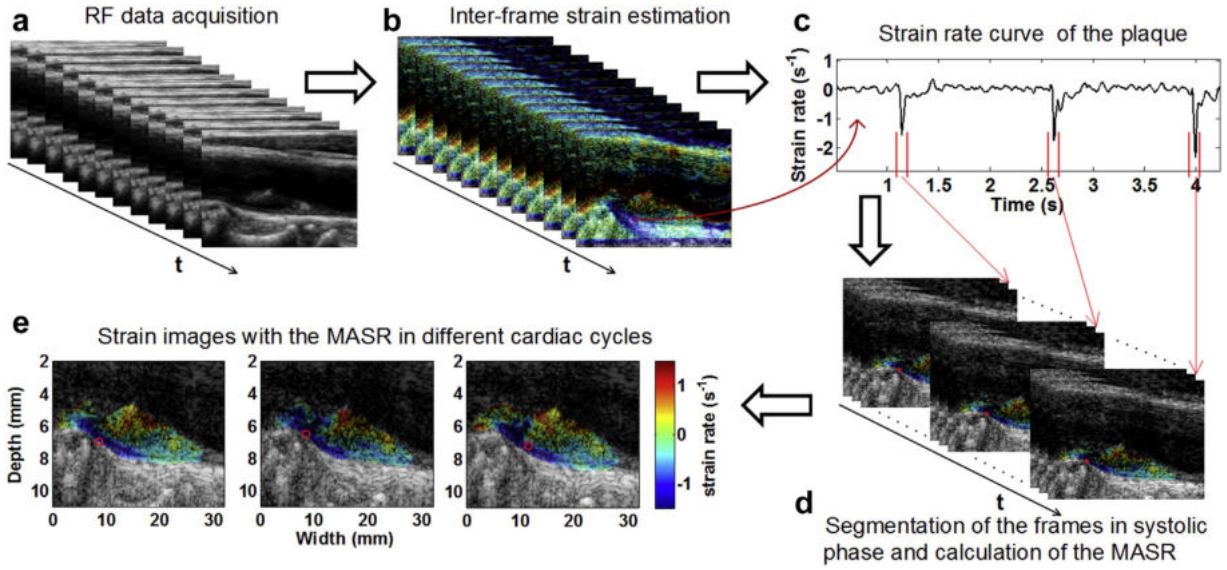

Fig. 1. Schematic of ultrasound data processing procedure. (a) RF data are acquired from the carotid plaques. (b) Inter-frame strains are estimated sequentially based on a two-step optical flow algorithm. (c) The strain rate curve of an arbitrary selected point inside the plaque is extracted, and the frames close to the peak value of the curve for each cardiac cycle are roughly identified, as indicated by the *red vertical lines*. The highest strain rate of the plaque typically appears in one of these frames. (d) Segmentation of the plaque is manually performed on the identified frames between *red vertical lines*, and the MASR inside the plaque is then calculated for each cardiac cycle. (e) The strain rate image corresponding to the MASR is obtained for each cardiac cycle and superimposed on the B-mode image. The locations of the highest strain rate are indicated by the *red circles*. RF = radiofrequency; MASR = maximum value of absolute strain rate.

flow algorithm with a tissue model of affine transformation (Pan et al. 2014a, 2015). A window size of about 1.7 × 1.3 mm^2 (height × width) and axial overlap of 90% in the optical flow method were used for all plaques. Only axial strain measurements were used in this study, because of their higher precision compared with lateral measurements. By normalization of the axial strain with the frame rate, the axial strain rate was obtained, representing the speed at which the deformation occurs.

Next, the axial strain rate as a function of time at an arbitrarily selected point (typically with high echogenicity or high signal-to-noise ratio [SNR]) inside the plaque was extracted (Fig. 1c), and frames close to the peak values of the curve for each cardiac cycle were roughly identified (indicated by the *red vertical lines* in Fig. 1c). The maximum inter-frame deformation of the plaque usually appeared around the identified frames. Therefore, to determine the exact frame in which the deformation rate was at the maximum, the plaques were manually segmented based on the B-mode and strain images corresponding to the identified frames (Fig. 1d). Segmentation of plaques was performed by a technician and confirmed by two senior reviewers, both blinded to the MRI results and ultrasound estimation. Afterward, the MASR inside the plaque was obtained for each cardiac cycle. The strain rate image corresponding to the MASR typically had the highest contrast and SNR in mapping tissue deformations, which may be correlated with the plaque composition distribution (Fig. 1e). As mentioned previously, high-risk features such as IPH and LRNC were shown to be softer than the stable features like CA and fibrous tissue, and consequently, vulnerable plaques may have higher strain rates than stable plaques. Therefore, the MASR, representing the highest absolute strain rate inside the plaque, was averaged over three to seven cardiac cycles and used as an indicator for plaque classification in this study.

MR image review

MR images were read by a junior reader and reviewed by a senior reader, both blinded to the ultrasound findings. The MR slices were reconstructed on the Philips MR workstation (Philips) using an algorithm of multiplanar reconstruction (MPR). Signal intensities of plaque tissues across the spatially matched 3-D-MERGE, SNAP and VISTA images were compared to identify the compositions of CA, IPH and LRNC according to published criteria (Cai et al. 2002; Saam et al. 2005; Yuan et al. 2001). LRNCs and vessel walls were manually segmented, and the ratio of LRNC relative to the vessel wall area in the transverse section was calculated. Plaques in which IPH was observed and/or

plaques with a maximum LRNC area ratio >20% were classified as vulnerable plaques (Underhill et al. 2010).

To match plaques in ultrasound images to the MR images, the carotid artery was divided into four segments—CCA, BF, ICA and ECA; a single plaque may be located in one or multiple segments of the carotid artery. Afterward, the plaque was further labeled as corresponding to the anterior wall, posterior wall or side wall of the selected segments. The ultrasound image and MR image were referred to the same plaque only if the plaque appeared in the same segments and on at least half of vessel walls in both image modalities, considering possible differences in orientation of plaques on vessel walls during manual comparison between MR and ultrasound images. Finally, plaques were classified into stable and vulnerable on the basis of compositional features determined by the MR review for validation of ultrasound carotid elastography.

Statistical analysis

Unless otherwise stated, patient characteristics and measurement values were presented as means ± standard deviations (SDs). Differences between stable plaques and vulnerable plaques were analyzed using a non-parametric Wilcoxon rank-sum test. Pearson's correlation coefficient was used to determine the correlation between ultrasound strain estimation and plaque thickness, as well as arterial stenosis. A p value < 0.05 was considered to indicate statistical significance. A receiver operating characteristic (ROC) curve was also generated to evaluate the performance of the MASR obtained from carotid elastography in separating vulnerable plaques from stable plaques by calculating the area under the ROC curve (AUC).

RESULTS

A typical example of a vulnerable plaque from the right ICA of a 70-y-old male patient is provided in Figure 2. The maximum thickness of the plaque is 3.01 mm, and the degree of stenosis is about 30%. IPH, a high-risk feature, is observed in the MR SNAP image (Fig. 2b), which suggests the plaque is vulnerable to rupture. CA is also identified within the plaque in the MR 3-D-MERGE image (Fig. 2c). For carotid elastography, the frame with the maximum deformation rate was determined for each cardiac cycle, and the corresponding strain rate images of the segmented plaque were superimposed on the reconstructed B-mode images, as illustrated in Figure 2 (d–f), for three consecutive cardiac cycles. Both high and low strain rate regions are observed inside the plaque, and the MASR was $3.44 \pm 0.66\ s^{-1}$ over three cardiac cycles. Regions with high strain rates may indicate the presence of high-risk features (such as IPH and large LCNCs), whereas low strain rate regions may be associated with low-risk features (such as CA and fibrous tissues). The strain rate curve at the maximum deformed location in the plaque (indicated by the *small red circle* in Fig. 2f) is plotted in Figure 2g, which reveals the consistency of the strain rate estimation over several consecutive cardiac cycles.

In Figure 3 is a representative case of stable plaque from the left BF of a 78-y-old male patient. The maximum thickness of the plaque is 3.21 mm, and the degree of arterial stenosis is about 32%, as measured by B-mode ultrasound (Fig. 3a). A large area of CA is identified on the MR 3-D-MERGE image (Fig. 3b), whereas IPH and LRNCs are absent, indicating a low-risk plaque. Similarly, the frame with the maximum deformation rate was identified, and the corresponding strain rate images of the segmented plaque superimposed on the B-mode images in three consecutive cardiac cycles are illustrated in Figure 3 (c–e). The strain rate at the maximum deformed location in the plaque (indicated by the *small red circle* in Fig. 3e) is plotted as a function of time in Figure 3f. Again, the strain rate distributions within the plaque in different cardiac cycles are similar, revealing good reproducibility of the strain measurement over several cardiac cycles. Unlike the vulnerable plaques, here the MASR is comparatively lower ($1.27 \pm 0.27\ s^{-1}$) over four cardiac cycles, which may be associated with the presence of the large area of CA as confirmed in the MR image (Fig. 3b).

Fifty-four patients met the acceptance criteria (maximum plaque thickness >2.5 mm) for further analysis. Among these patients, 14 were excluded because major parts of their plaques were located on the side walls and, thus, were difficult to process in longitudinal views. Another 11 were excluded for poor image quality in either ultrasound imaging or MRI. In total, 46 plaques from 29 patients were chosen. The clinical characteristics for one of the included patients were not available; the characteristics of the remaining 28 patients are summarized in Table 2. Eighteen patients were hypertensive and taking anti-hypertensive medications. A small portion of the patients were smokers (6 of 28 patients). Of the 46 plaques, 19 were identified as stable, and the other 27 plaques were classified as vulnerable based on MRI. The characteristics of the stable and vulnerable plaques as measured in ultrasound and MRI are summarized in Table 3. There were no significant differences in maximum plaque thickness and arterial stenosis between the stable and vulnerable plaques (both $p > 0.9$). And there is no significant correlation between the MASR and maximum plaque thickness ($r = 0.278$, 95% confidence interval [CI]: −0.013 to 0.526, $p > 0.05$), but there was a significant positive correlation between the MASR and arterial stenosis ($r = 0.336$, 95% CI: 0.051–0.571, $p = 0.02$). However, the MASR derived from carotid

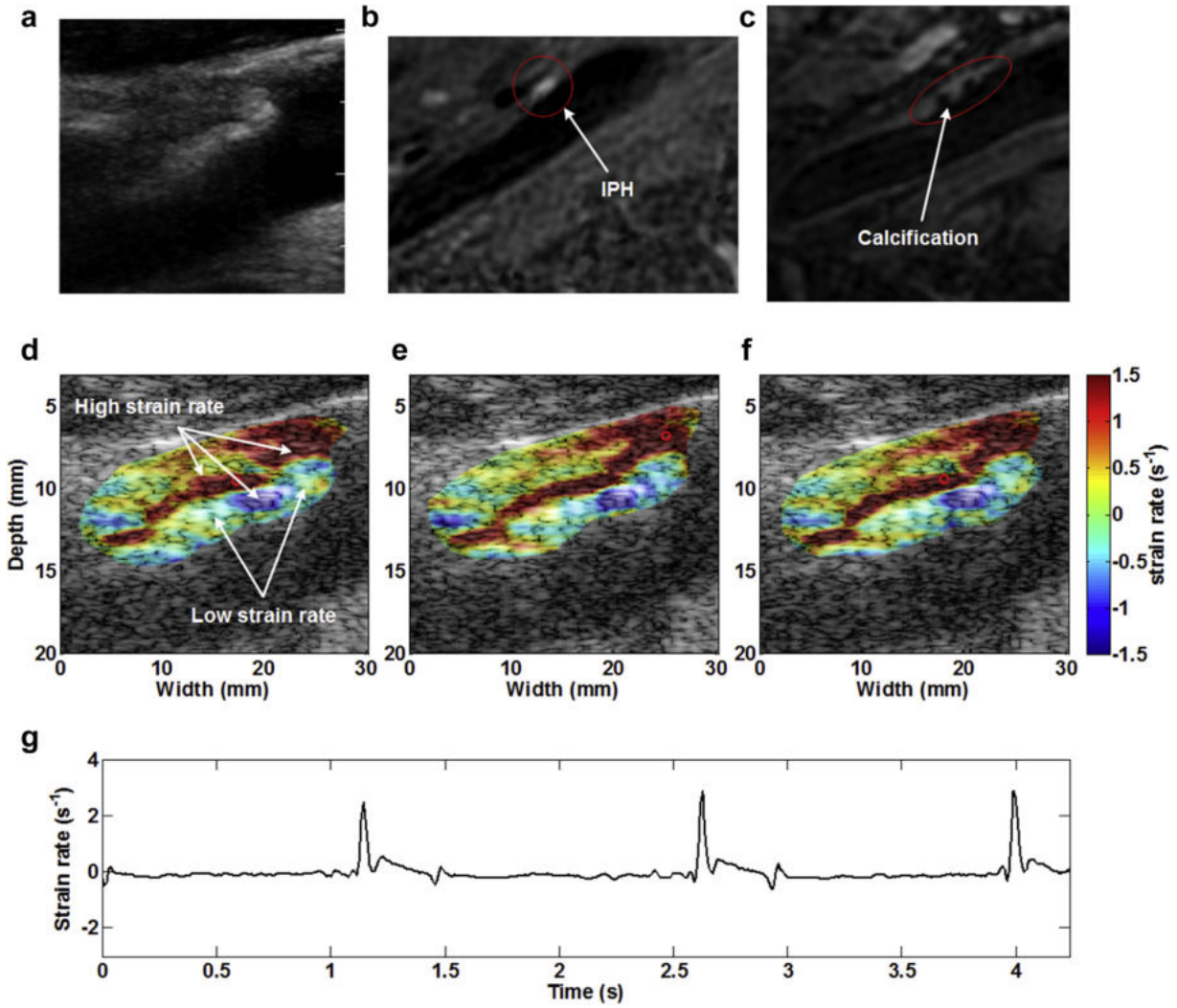

Fig. 2. Typical case of vulnerable plaque in the right ICA of a 70-y-old male patient. (a) Ultrasound B-mode image of the plaque. (b) MR SNAP image, with the *bright region inside the red circle* indicating the presence of IPH. (c) 3-D-MERGE image, with the *dark region inside the red circle* indicating the presence of CA. (d–f) Strain rate images of the segmented plaque superimposed on the reconstructed B-mode images in the systolic phases of three consecutive cardiac cycles. The *small red circles* indicate the locations of peak strain rate over the plaque. Both high and low strain rate regions are observed inside the plaque and the MASR is $3.44 \pm 0.66\ s^{-1}$. (g) Strain rate at the maximum deformed location (indicated by the *small red circle* in e) as a function of time. ICA = internal carotid artery; MR = magnetic resonance; SNAP = simultaneous non-contrast angiography and intra-plaque hemorrhage; IPH = intra-plaque hemorrhage; 3-D MERGE = 3-D motion sensitized driven equilibrium prepared rapid gradient echo; CA = calcification; MASR = maximum value of absolute strain rate.

elastography was significantly higher in vulnerable plaques ($2.15 \pm 0.79\ s^{-1}$) than in stable plaques ($1.21 \pm 0.37\ s^{-1}$, $p < 0.0001$), as indicated in Figure 4 and Table 3. The ROC curve for MASR in the detection of vulnerable plaques is provided in Figure 5, and the AUC is 0.848 (95% CI: 0.737–0.959). A sensitivity (*i.e.*, percentage of correctly identified vulnerable plaques among all vulnerable plaques) of 81.48% and specificity (*i.e.*, percentage of correctly identified stable plaques among all stable plaques) of 89.47% were obtained at the point with maximum overall accuracy (*i.e.*, percentage of the sum of correctly identified stable and vulnerable plaques with respect to total plaque sample size, 84.78%) for a discriminating threshold of $1.45\ s^{-1}$.

DISCUSSION

Ultrasound methods for identification of vulnerable plaques are urgently needed to prevent ischemic cardiovascular events. For this reason, carotid elastography has been developed to characterize the mechanical properties and composition of atherosclerotic plaques by

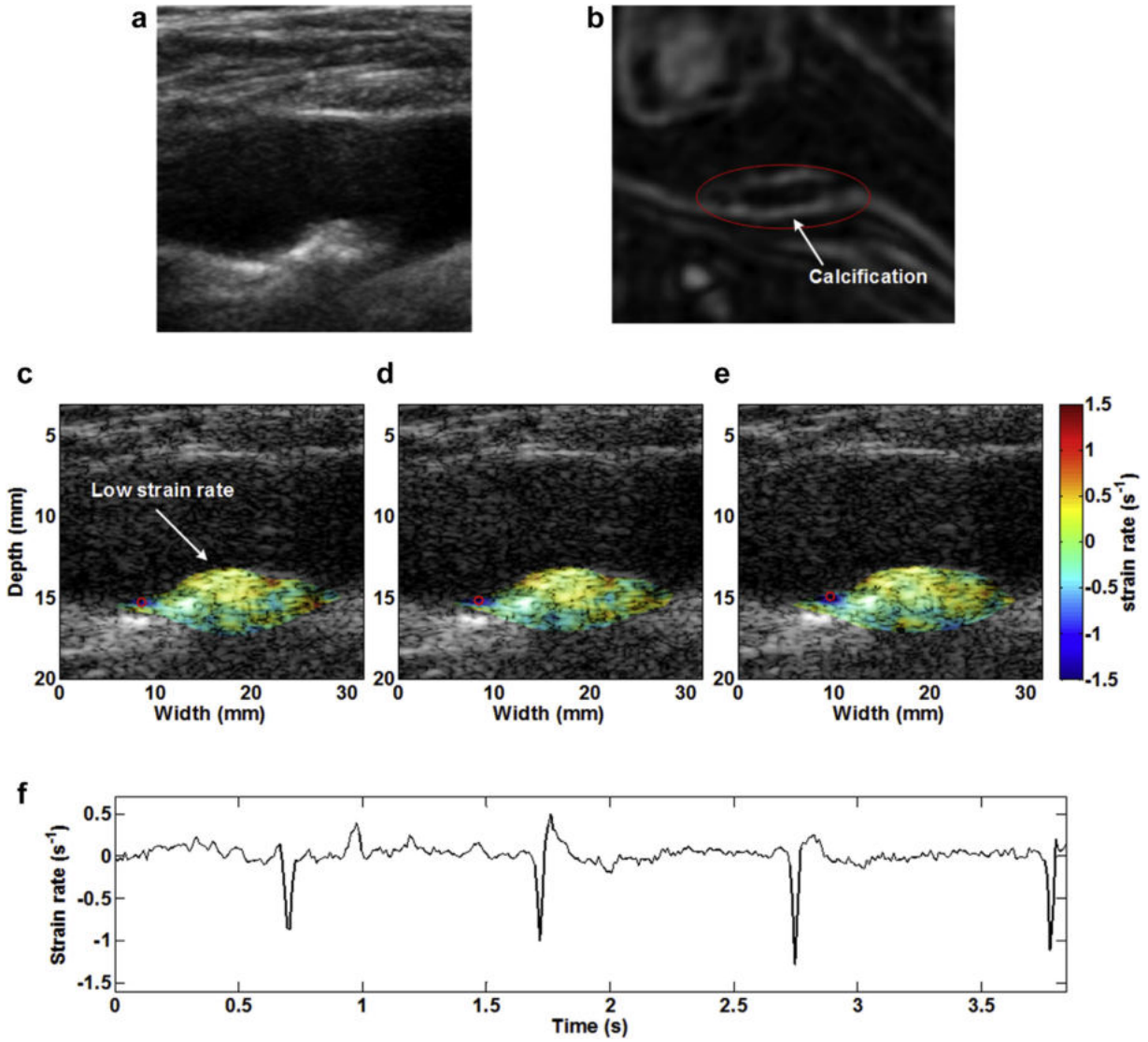

Fig. 3. Typical case of stable plaque in the left BF of a 78-y-old male patient. (a) Ultrasound B-mode image of the plaque. (b) 3-D-MERGE image, with the *dark region inside the red circle* indicating the presence of CA. (c–e) Strain rate images of the segmented plaque superimposed on the reconstructed B-mode images in the systolic phases of three consecutive cardiac cycles. The *small red circles* indicate the locations of peak strain rate over the plaque. The MASR is comparatively low ($1.27 \pm 0.27\ s^{-1}$). (f) The strain rate at the maximum deformed location (indicated by the *small red circle* in e) as a function of time. BF = bifurcation; 3-D MERGE = 3-D motion sensitized driven equilibrium prepared rapid gradient echo; CA = calcification; MASR = maximum value of absolute strain rate.

measuring the strain (rate) distribution of the plaques at different intraluminal blood pressures. Different plaque compositions have been reported to have different strain values in IVUS elastography, with higher strain being associated with vulnerable features, such as IPH and LRNCs (de Korte et al. 2000; Kanai et al. 2003; Schaar et al. 2001). In this study, the *in vivo* capability of carotid elastography to identify vulnerable plaques in human carotid arteries was evaluated using MRI as reference. We found that vulnerable plaques had significantly larger local deformation rates (higher local strain rate) than stable plaques ($p < 0.0001$), in good agreement with previous findings from IVUS elastography. The MASR, derived from the strain measurement and representing the highest local strain rate inside the plaque, performs relatively well in differentiating between vulnerable and stable plaques of carotid arteries as determined by MRI (AUC = 0.848). These results may provide important *in vivo* validation of the usefulness of carotid elastography and indicate that carotid elastography is a promising tool for assessment of atherosclerotic plaques.

Table 2. Characteristics of patients involved in this study

Parameter	Value
Age (y)	74 ± 5
Sex (M/F)	23/5
Body mass index (kg/m^2)	23.6 ± 2.8
Brachial DBP (mm Hg)	71 ± 11
Brachial SBP (mm Hg)	135 ± 15
Brachial pulse pressure (mm Hg)	64 ± 16
Ankle SBP (mm Hg)	153 ± 17
Ankle brachial index	1.14 ± 0.13
Hypertension	18 (64.3%)
Smoking history	6 (21.43%)
High-density lipoprotein (mmol/L)	1.42 ± 0.38
Low-density lipoprotein (mmol/L)	2.69 ± 0.97
Triglycerides (mmol/L)	1.29 ± 0.54
Total cholesterol (mmol/L)	4.63 ± 0.91
Blood sugar (mmol/L)	5.60 ± 0.68

DBP = diastolic blood pressure; SBP = systolic blood pressure.

The strain image of the plaque is a measurement of deformation distribution and may be correlated with composition distribution. In this study, compositional features of CA, IPH and LRNC were characterized *in vivo* by MRI and compared with the ultrasound strain measurements. Because the high-risk features such as IPH and large LRNCs are softer compositions, regions of high strain rate may correspond to locations of IPH and large LRNCs that are likely to rupture (Fig. 2), as validated in the MR images, whereas regions with low strain rates may be associated with the presence of stiffer features such as CA and fibrous tissues (Figs. 2 and 3). Nevertheless, the exact spatial correlation between plaque compositions and strain distribution will require accurate registration between ultrasound images and MR images, and thus, the relationship between the locations of MASR and plaque composition is absent. Therefore, in this study, the quantitative index of MASR does not correlate with the exact plaque composition distribution, but higher MASR values may reveal the presence of large LRNCs and/or IPH, indicating vulnerability of plaques.

Table 3. Characteristics of stable and vulnerable plaques derived from ultrasound imaging and MRI

	Stable plaques (n = 19)	Vulnerable plaques (n = 27)	*p* Value
Ultrasound characteristics			
Maximum thickness (mm)	2.78 ± 0.64	2.95 ± 0.96	0.92
Stenosis (%)*	29.0 ± 5.9	30.9 ± 10.3	0.97
MASR (s^{-1})	1.21 ± 0.37	2.15 ± 0.79	<0.0001
MRI characteristics			
Intra-plaque hemorrhage	0 (0.0%)	22 (81.5%)	—
Lipid-rich necrotic core	16 (84.2%)	26 (96.3%)	—
Calcification	15 (79.0%)	25 (92.6%)	—

MRI = magnetic resonance imaging; MASR = maximum value of absolute strain rate.

* Stenosis is defined as the percentage reduction in luminal diameter.

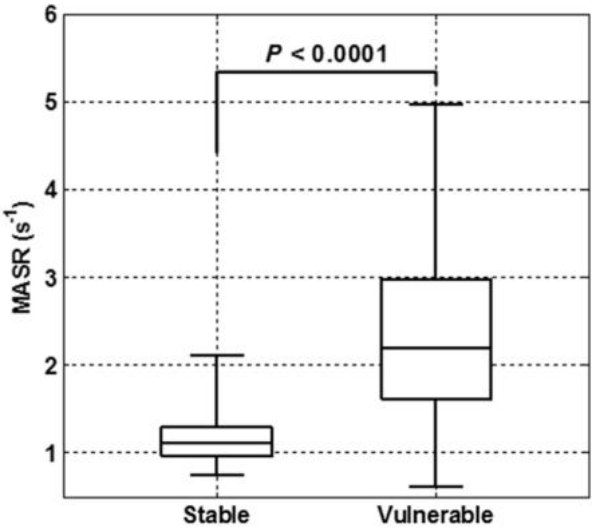

Fig. 4. MASR of stable and vulnerable plaques. The plotted whiskers extend to the minimum and maximum values. MASR = maximum value of absolute strain rate.

By comparing the strain rate images of vulnerable and stable plaques (as illustrated for the examples in Figs. 2 and 3), it is observed that the strain rate distribution of the vulnerable plaque commonly appears to be less uniform than that of the stable plaque. Therefore, the uniformity of the strain rate distribution may also provide important information for plaque classification, which is part of our ongoing studies. In addition, both positive (stretching) and negative (compression) strain rates are found in most plaques in the systolic phase, when the

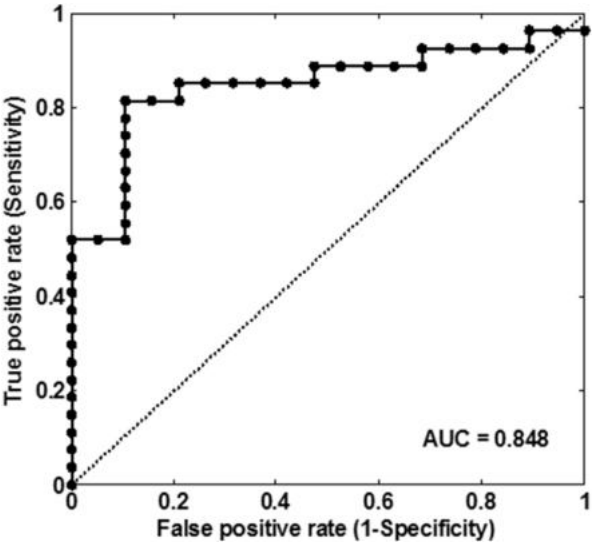

Fig. 5. Receiver operating characteristic curve for the MASR in discriminating between the stable and vulnerable plaques. AUC = area under the curve; MASR = maximum value of absolute strain rate.

arteries are distending. This could be explained by the complicated hemodynamics and boundary conditions in the presence of plaques, especially for the plaques inducing severe stenosis, as well as the complex mechanical properties associated with different plaque compositions. Therefore, blood flow and hemodynamic information will also be helpful in quantifying plaque properties. Overall, according to the observations in this study, features of vulnerable plaques in elastography typically consist of a high local strain rate and spatially non-uniform strain rate distributions; in contrast, stable plaques typically are associated with low local strain rate and relatively uniform strain rate distributions.

Although several research groups have been working on non-invasive vascular elastography or strain imaging, *in vivo* validation of carotid elastography using MRI was only recently performed by Naim et al. (2013). In their study, ultrasound RF signals were acquired on an ES500 RP system (Ultrasonix, Vancouver, Canada), and MRI was performed on a 1.5-T MR scanner (Siemens, Avanto, Erlangen, Germany). Four strain parameters were obtained from the spatial average of the axial strain on the whole segmented plaque, and the association between strain parameters and plaque characterizations was assessed. They reported that carotid elastography can detect the presence of lipid cores with high sensitivity and moderate specificity; but strain in plaques with lipid cores was found to be significantly lower than that in plaques without lipid cores, which was in contrast to previous findings in IVUS elastography of the coronary, iliac and femoral arteries. As explained by Naim et al. (2013), this may be due to the damping effect of the lipid core embedded in a large plaque and the spatial averaging of the strain parameters on the whole plaque. In our study, strain estimation was performed on the RF signals acquired with a Philips iU22 ultrasound system, and the MRI validation was conducted with a 3.0-T MR scanner with a 36-channel coil. Instead of spatially averaging the strain parameters, we used the highest local strain rate within the plaque as a simple parameter (*i.e.*, the MASR) and found that plaques with IPH and/or larger LRNCs (high-risk features) had significantly higher local strain rates. Consequently, by use of the MASR, vulnerable plaques or high-risk patients can be successfully identified. Our results are in accordance with that high-risk compositional features such as IPH and LRNCs are softer than low-risk components, and are also consistent with the previous findings in IVUS elastography that had been validated histologically. Because of the complicated compositions of vulnerable plaques, the localized regions with elevated strain (rate) may indicate the potentially vulnerable locations, which might also explain the effectiveness of the local strain parameter in our study.

It is observed that multiple high-strain-rate regions with similar strain rate values may exist inside a single plaque, and consequently, the highest absolute strain rate may not always appear at the same spatial location in different cardiac cycles, as illustrated in Figure 2 (d–f). In such cases, the highest absolute strain rates, even those derived from different regions of the plaque, are similar, which, would hardly affect calculation of the averaged MASR over several cardiac cycles. On the other hand, no significant difference was found in plaque thickness or arterial stenosis between stable and vulnerable plaques in this study, in accordance with previous reports (Falk et al. 1995). In ultrasound B-mode images, high echogenicity region of the plaques is conventionally considered as an indicator of CA and regarded as a stable feature. However, high-risk features (*e.g.*, IPH and LRNC) commonly appear in plaques alongside with the CAs (of 27 vulnerable plaques, 25 had CAs) (Table 3), which interferes with the interpretation of plaque stabilization when using only B-mode images. Therefore, given that the relative stiffness can be provided by carotid elastography, a combination of B-mode images and strain images might enhance the characterization of plaques and further improve diagnostic accuracy.

The long-term goal of our study is to develop multimodality imaging-based biomarkers for carotid plaque characterization. Because of its advantages of cost-effectiveness, fast scan speed, real-time capability and widespread availability, ultrasound imaging could be used for screening, monitoring and follow-up in large populations. For patients determined to be at high risk by ultrasound imaging, MR scanning would be recommended for accurate characterization of plaques and, consequently, optimization of clinical decision making on prevention or treatment. In this aspect, the exact composition of the plaques estimated from carotid elastography or ultrasound imaging may not be necessary. Thus, here we propose the MASR as a simple quantitative index in the detection of vulnerable plaques, instead of the assessment of exact plaque composition (which requires accurate registration between ultrasound imaging and MRI for validation, as previously discussed).

Considering that the strain distribution of plaque is determined by material properties and external force (*i.e.*, blood pressure), the impact of intraluminal blood pressure should be taken into account. Because strain was estimated between adjacent frames, one strategy is to normalize the inter-frame strain with respect to the corresponding inter-frame pressure difference (Maurice et al. 2008). Inter-frame pressure was approximated as the brachial pulse pressure divided by the number of frames between end-diastole and peak systole, as done in a previous study. In this study, corresponding to the MASR, the maximum value of absolute strain (MAS)

for each plaque was normalized based on this strategy to generate a mechanical index related to the incremental Young's modulus, and the results are illustrated in Figures 6 and 7. Significant differences in pressure-normalized MAS values can also be found between stable and vulnerable plaques with $p = 0.0011$ (Fig. 6), whereas the AUC for detecting vulnerable plaques is 0.787 (95% CI: 0.656–0.919) (Fig. 7), indicating lower discriminating performance compared with the non-pressure-normalized indicator MASR. Such results may be explained as follows: As reliable methods for direct and non-invasive determination of carotid blood pressure are currently unavailable, brachial cuff blood pressure is typically measured as an alternative, which could introduce bias in the normalization. Additionally, considering the somewhat lower accuracy of the brachial blood pressure measurement, the accuracy of the pressure-normalized MAS might also be affected. Another major source of error comes from the determination of inter-frame pressure difference. Because only the systolic and diastolic blood pressures are recorded instead of the complete pressure waveform, the inter-frame blood pressure can only be calculated based on the assumption that blood pressure increases linearly from end-diastole to peak systole, which however is not the case *in vivo* and is deemed to be overly simple. All of the aforementioned reasons may potentially lead to decreased performance of pressure-normalized strain in detecting vulnerable plaques.

Despite the promising performance of carotid elastography indicated by the results, this study has several limitations. The ultrasound data were acquired mainly from longitudinal imaging views of the arteries, where

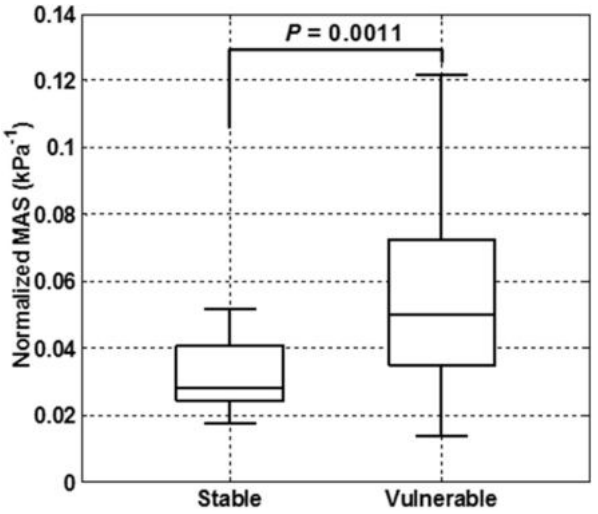

Fig. 6. Pressure-normalized MAS for stable and vulnerable plaques. The plotted whiskers extend to the minimum and maximum values. MAS = maximum value of absolute strain.

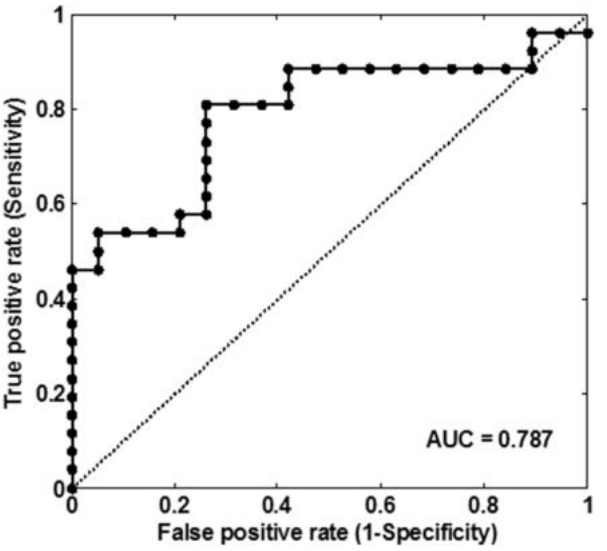

Fig. 7. Receiver operating characteristic curve for the pressure-normalized MAS in discriminating between the stable and vulnerable plaques. AUC = area under the curve; MAS = maximum value of absolute strain.

the axial strain is closely aligned with the radial strain of the plaques (de Korte et al. 2011). However, longitudinal imaging views are not always capable of covering all the plaques, and thus, those plaques located mainly at the side walls were not included in the present study. To overcome this limitation, strain imaging must be performed in transverse imaging views. As mentioned in the Introduction section, lateral strain estimation is required to construct the radial and circumferential strain of the arteries in the transverse imaging views, which poses a certain level of difficulty as strain estimation in the lateral direction is less reliable (de Korte et al. 2011). Therefore, only the axial strain (closely corresponding to the radial strain in the longitudinal imaging views) was considered in the present study. To further improve the performance of carotid elastography, accurate estimation of all components of the displacement vector and strain tensor in the transverse imaging views would be preferable. One way to achieve this is the spatial angular compounding technique, in which the lateral displacement and strain are constructed from the axial displacement estimated on the RF signals acquired at different transmitting angles (Hansen et al. 2009, 2014; Nakagawa et al. 2004; Poree et al. 2015). With more robust lateral displacement estimation, accumulated strain in the entire systolic phase in both the axial and lateral directions might also be obtained to provide a higher contrast of the strain images in revealing different plaque compositions.

Segmentation of the plaques was manually implemented currently to reduce the noise in strain estimation at the boundary. However, the manual segmentation procedure appears to influence, more or less, the final

identification of the MASR, which might be considered as another limitation of the present study. To minimize human intervention in this study, segmentation results were determined by two experienced reviewers blinded to the strain estimation procedure. Another way to reduce the influence of segmentation is to develop indicators representing overall strain distribution inside the plaque instead of a single MASR, and such work is ongoing. Additionally, the imaging in the present study was performed using a linear array transducer (L9-3) with a relatively low center frequency. By use of a higher-frequency probe, higher spatial resolution of both the B-mode and strain (rate) images can be achieved. Furthermore, sample size is limited for statistical analysis; therefore, investigations involving larger numbers of patients might be warranted.

Another limitation is that we considered only the presence of IPH and area of LRNC in the MRI analysis; other features of vulnerable plaques, such as fibrous cap rupture, inflammation and neovascularization, were not included. Both IPH and LRNC are compositional features of plaques and have been found in *ex vivo* experiments to differ in stiffness from other features of stability such as CA and fibrous tissue (Chai et al. 2013; Lee et al. 1992). The MASR derived from carotid elastography is also related to the stiffness of plaques and, therefore, is linked to the MRI results based on the compositional feature of IPH and LRNC. More recently, the association between plaque strain and intra-plaque neovascularization was reported, further confirming the potential of carotid elastography in plaque characterization (Zhang et al. 2015). Additionally, the plaques were simply classified as either stable or vulnerable on the basis of MR image review in the present study. In the future, a quantitative score of rupture risk derived from a more comprehensive MR image review may be used, and the relationship between the MASR (or other parameters derived from carotid elastography) and different degrees of rupture risk may be established.

CONCLUSIONS

In this study, the *in vivo* capability of carotid elastography in the characterization and classification of atherosclerotic plaques was evaluated using magnetic resonance imaging as the reference. Statistical analysis revealed that the maximum value of absolute strain rate (MASR), a simple and quantitative index, was significantly higher in vulnerable plaques than in stable plaques. ROC analysis revealed the good performance of carotid elastography in detecting high-risk plaques (determined by MRI) using the MASR as an indicator. Therefore, carotid elastography may serve as a simple and non-invasive tool for assessment of atherosclerosis and may be useful for screening large populations in early identification of high-risk patients.

Acknowledgments—This study was supported in part by the National Natural Science Foundation of China (61271131, 61322101 and 81471665); the Specialized Research Fund for the Doctoral Program of Higher Education of China (20130002110061); the Shenzhen Science and Technology Plan Project (JCYJ20140417115840275); and the Tsinghua University Initiative Scientific Research Program. The authors thank Le He, Center for Biomedical Imaging Research (CBIR), Tsinghua University, for her assistance in patient scanning and data collection. The authors also thank Zechen Zhou at CBIR for helpful discussion.

REFERENCES

Apostolakis IZ, Nandlall SD, Konofagou EE. Piecewise pulse wave imaging (pPWI) for detection and monitoring of focal vascular disease in murine aortas and carotids *in vivo*. IEEE Trans Med Imaging. in press, 10.1109/TMI.2015.2453194; 2015.

Balu N, Yarnykh VL, Chu BC, Wang JN, Hatsukami T, Yuan C. Carotid plaque assessment using fast 3-D isotropic resolution black-blood MRI. Magn Reson Med 2011;65:627–637.

Bonnefous O, Brevannes L, Denis E, Sananes JC, Montaudon M, Laurent FH, Drouillard J. New noninvasive echographic technique for arterial wall characterization. Radiology 1996;201:1129.

Cai JM, Hastukami TS, Ferguson MS, Small R, Polissar NL, Yuan C. Classification of human carotid atherosclerotic lesions with *in vivo* multicontrast magnetic resonance imaging. Circulation 2002;106:1368–1373.

Chai CK, Akyildiz AC, Speelman L, Gijsen FJH, Oomens CWJ, van Sambeek M, van der Lugt A, Baaijens FPT. Local axial compressive mechanical properties of human carotid atherosclerotic plaques: Characterisation by indentation test and inverse finite element analysis. J Biomech 2013;46:1759–1766.

Chu BC, Zhao XQ, Saam T, Yarnykh VL, Kerwin WS, Flemming KD, Huston J, Insull W, Morrisett JD, Rand SD, DeMarco KJ, Polissar NL, Balu N, Cai JM, Kampschulte A, Hatsukami TS, Yuan C. Feasibility of *in vivo*, multicontrast-weighted MR imaging of carotid atherosclerosis for multicenter studies. J Magn Reson Imaging 2005;21:809–817.

Czernuszewicz TJ, Homeister JW, Caughey MC, Farber MA, Fulton JJ, Ford PF, Marston WA, Vallabhaneni R, Nichols TC, Gallippi CM. Non-invasive *in vivo* characterization of human carotid plaques with acoustic radiation force impulse ultrasound: Comparison with histology after endarterectomy. Ultrasound Med Biol 2015;41:685–697.

de Korte CL, Cespedes EI, vanderSteen AFW, Lancee CT. Intravascular elasticity imaging using ultrasound: Feasibility studies in phantoms. Ultrasound Med Biol 1997;23:735–746.

de Korte CL, Pasterkamp G, van der Steen AFW, Woutman HA, Bom N. Characterization of plaque components with intravascular ultrasound elastography in human femoral and coronary arteries *in vitro*. Circulation 2000;102:617–623.

de Korte CL, Hansen HHG, van der Steen AFW. Vascular ultrasound for atherosclerosis imaging. Interface Focus 2011;1:565–575.

Doherty J, Dahl J, Kranz P, El Husseini N, Chang H, Chen N, Allen J, Ham K, Trahey G. Comparison of acoustic radiation force impulse imaging derived carotid plaque stiffness with spatially registered MRI determined composition. IEEE Trans Med Imaging. in press, 10.1109/TMI.2015.2432797; 2015.

Dong L, Underhill HR, Yu W, Ota H, Hatsukami TS, Gao TL, Zhang Z, Oikawa M, Zhao X, Yuan C. Geometric and compositional appearance of atheroma in an angiographically normal carotid artery in patients with atherosclerosis. Am J Neuroradiol 2010;31:311–316.

Falk E, Shah PK, Fuster V. Coronary plaque disruption. Circulation 1995;92:657–671.

Fan ZY, Zhang ZL, Chung YC, Weale P, Zuehlsdorff S, Carr J, Li DBA. Carotid arterial wall MRI at 3 T using 3-D variable-flip-angle turbo spin-echo (TSE) with flow-sensitive dephasing (FSD). J Magn Reson Imaging 2010;31:645–654.

Finn AV, Nakano M, Narula J, Kolodgie FD, Virmani R. Concept of vulnerable/unstable plaque. Arterioscler Thromb Vasc Biol 2010; 30:1282–1292.
Golemati S, Gastounioti A, Nikita KS. Toward novel noninvasive and low-cost markers for predicting strokes in asymptomatic carotid atherosclerosis: The role of ultrasound image analysis. IEEE Trans Biomed Eng 2013;60:652–658.
Grant EG, Benson CB, Moneta GL, Alexandrov AV, Baker JD, Bluth EI, Carroll BA, Eliasziw M, Gocke J, Hertzberg BS, Katarick S, Needleman L, Pellerito J, Polak JF, Rholl KS, Wooster DL, Zierler E. Carotid artery stenosis: Grayscale and Doppler ultrasound diagnosis—Society of Radiologists in Ultrasound Consensus Conference. Radiology 2003;19:190–198.
Hansen HHG, Lopata RGP, de Korte CL. Noninvasive carotid strain imaging using angular compounding at large beam steered angles: Validation in vessel phantoms. IEEE Trans Med Imaging 2009;28: 872–880.
Hansen HHG, Lopata RGP, Idzenga T, de Korte CL. An angular compounding technique using displacement projection for noninvasive ultrasound strain imaging of vessel cross-sections. Ultrasound Med Biol 2010a;36:1947–1956.
Hansen HHG, Lopata RGP, Idzenga T, de Korte CL. Full 2-D displacement vector and strain tensor estimation for superficial tissue using beam-steered ultrasound imaging. Phys Med Biol 2010b;55: 3201–3218.
Hansen HHG, Saris A, Vaka NR, Nillesen MM, de Korte CL. Ultrafast vascular strain compounding using plane wave transmission. J Biomech 2014;47:815–823.
Hasegawa H, Kanai H. Simultaneous imaging of artery-wall strain and blood flow by high frame rate acquisition of RF signals. IEEE Trans Ultrason Ferroelectr Freq Control 2008;55:2626–2639.
Huang L, He Q, Zhao X, Huang M, Luo J. A new ultrasound imaging indicator for vulnerability evaluation of carotid atherosclerotic plaques. Proc IEEE Int Ultrason Symp 2014;5–8.
Kanai H, Hasegawa H, Ichiki M, Tezuka F, Koiwa Y. Elasticity imaging of atheroma with transcutaneous ultrasound preliminary study. Circulation 2003;107:3018–3021.
Kim K, Huang SW, Hall TL, Witte RS, Chenevert TL, O'Donnell M. Arterial vulnerable plaque characterization using ultrasound-induced thermal strain imaging (TSI). IEEE Trans Biomed Eng 2008;55:171–180.
Korukonda S, Doyley MM. Visualizing the radial and circumferential strain distribution within vessel phantoms using synthetic-aperture ultrasound elastography. IEEE Trans Ultrason Ferroelectr Freq Control 2012;59:1639–1653.
Korukonda S, Nayak R, Carson N, Schifitto G, Dogra V, Doyley MM. Noninvasive vascular elastography using plane-wave and sparse-array imaging. IEEE Trans Ultrason Ferroelectr Freq Control 2013;60:332–342.
Larsson M, Verbrugghe P, Smoljkic M, Verhoeven J, Heyde B, Famaey N, Herijgers P, D'Hooge J. Strain assessment in the carotid artery wall using ultrasound speckle tracking: Validation in a sheep model. Phys Med Biol 2015;60:1107–1123.
Lee RT, Richardson SG, Loree HM, Grodzinsky AJ, Gharib SA, Schoen FJ, Pandian N. Prediction of mechanical-properties of human atherosclerotic tissue by high-frequency intravascular ultrasound imaging: An *in vitro* study. Arterioscler Thromb 1992;12:1–5.
Li RX, Apostolakis IZ, McKinsey JF, Connolly ES, Konofagou EE. *In vivo* characterization of atherosclerotic plaques using pulse wave imaging-based stiffness maps. Presented at the IEEE International Ultrasonics Symposium, Chicago, IL, USA, 3–6 September, 2014.
Lopata RGP, Peters MFJ, Nijs J, Oomens CWJ, Rutten MCM, van de Vosse FN. Vascular elastography: A validation study. Ultrasound Med Biol 2014;40:1882–1895.
Luo J, Pan X, Huang L, Tao S, Huang M, Zhao X, He L, Yuan C, Bai J. A feasibility study of ultrasound B-mode and strain imaging for risk assessment of carotid atherosclerotic plaques validated by magnetic resonance imaging. Proc IEEE Int Ultrason Symp 2013;565–568.
Maurice RL, Ohayon J, Fretigny Y, Bertrand M, Soulez G, Cloutier G. Noninvasive vascular elastography: Theoretical framework. IEEE Trans Med Imaging 2004;23:164–180.
Maurice RL, Soulez G, Giroux MF, Cloutier G. Noninvasive vascular elastography for carotid artery characterization on subjects without previous history of atherosclerosis. Med Phys 2008;35:3436–3443.
Mendel T, Popow J, Hier DB, Czlonkowska A. Advanced atherosclerosis of the aortic arch is uncommon in ischemic stroke: An autopsy study. Neurol Res 2002;24:491–494.
Naim C, Cloutier G, Mercure E, Destrempes F, Qin Z, El-Abyad W, Lanthier S, Giroux MF, Soulez G. Characterisation of carotid plaques with ultrasound elastography: Feasibility and correlation with high-resolution magnetic resonance imaging. Eur Radiol 2013;23:2030–2041.
Nakagawa N, Hasegawa H, Kanai H. Cross-sectional elasticity imaging of carotid arterial wall in short-axis plane by transcutaneous ultrasound. Jpn J Appl Phys 2004;43:3220–3226.
National Center for Cardiovascular Diseases, China. Report on cardiovascular diseases in China (2013); 2013.
Naylor AR. Time to rethink management strategies in asymptomatic carotid artery disease. Nat Rev Cardiol 2012;9:116–124.
Ophir J, Garra B, Kallel F, Konofagou E, Krouskop T, Righetti R, Varghese T. Elastographic imaging. Ultrasound Med Biol 2000;26: S23–S29.
Pan X, Gao J, Tao S, Liu K, Bai J, Luo J. A two-step optical flow method for strain estimation in elastography: Simulation and phantom study. Ultrasonics 2014a;54:990–996.
Pan X, Huang L, Huang M, Zhao X, He L, Yuan C, Bai J, Luo J. A feasibility study of carotid elastography for risk assessment of atherosclerotic plaques validated by magnetic resonance imaging. Proc SPIE 2014b;9040:904002.
Pan X, Liu K, Shao J, Gao J, Huang L, Bai J, Luo J. Performance comparison of rigid and affine models for motion estimation using ultrasound radio-frequency signals. IEEE Trans Ultrason Ferroelectr Freq Control 2015;62:1928–1943.
Phan BAP, Chu BC, Polissar N, Hatsukami TS, Yuan C, Zhao XQ. Association of high-density lipoprotein levels and carotid atherosclerotic plaque characteristics by magnetic resonance imaging. Int J Cardiovasc Imaging 2007;23:337–342.
Poree J, Garcia D, Chayer B, Ohayon J, Cloutier G. Non-invasive vascular elastography with plane strain incompressibility assumption using ultrafast coherent compound plane wave imaging. IEEE Trans Med Imaging 2015;34:2618–2631.
Ribbers H, Lopata RGP, Holewijn S, Pasterkamp G, Blankensteijn JD, De Korte CL. Noninvasive two-dimensional strain imaging of arteries: Validation in phantoms and preliminary experience in carotid arteries *in vivo*. Ultrasound Med Biol 2007;33:530–540.
Richards MS, Doyley MM. Non-rigid image registration based strain estimator for intravascular ultrasound elastography. Ultrasound Med Biol 2013;39:515–533.
Saam T, Ferguson MS, Yarnykh VL, Takaya N, Xu D, Polissar NL, Hatsukami TS, Yuan C. Quantitative evaluation of carotid plaque composition by *in vivo* MRI. Arterioscler Thromb Vasc Biol 2005; 25:234–239.
Saam T, Hatsukami TS, Yarnykh VL, Hayes CE, Underhill H, Chu BC, Takaya N, Cai JM, Kerwin WS, Xu DX, Polissar NL, Neradilek B, Hamar WK, Maki J, Shaw DW, Buck RJ, Wyman B, Yuan C. Reader and platform reproducibility for quantitative assessment of carotid atherosclerotic plaque using 1.5 T Siemens, Philips, and general electric scanners. J Magn Reson Imaging 2007;26:344–352.
Saam T, Underhill HR, Chu BC, Takaya N, Cai JM, Polissar NL, Yuan C, Hatsukami TS. Prevalence of American Heart Association type VI carotid atherosclerotic lesions identified by magnetic resonance imaging for different levels of stenosis as measured by duplex ultrasound. J Am Coll Cardiol 2008;51:1014–1021.
Schaar JA, De Korte CL, Mastik F, Strijder C, Pasterkamp G, Van der Steen AF. Vulnerable plaque detection with intravascular elastography: A sensitivity and specificity study. Circulation 2001;104:459.
Shapo BM, Crowe JR, Erkamp R, Emelianov SY, Eberle MJ, O'Donnell M. Strain imaging of coronary arteries with intraluminal ultrasound: Experiments on an inhomogenous phantom. Ultrason Imaging 1996;18:173–191.
Shi HR, Mitchell CC, McCormick M, Kliewer MA, Dempsey RJ, Varghese T. Preliminary *in vivo* atherosclerotic carotid plaque

characterization using the accumulated axial strain and relative lateral shift strain indices. Phys Med Biol 2008;53:6377–6394.
Streifler JY. Asymptomatic carotid stenosis: Intervention or just stick to medical therapy—The case for medical therapy. J Neural Transm 2011;118:637–640.
Underhill HR, Yuan C, Zhao XQ, Kraiss LW, Parker DL, Saam T, Chu B, Takaya N, Liu F, Polissar NL, Neradilek B, Raichlen JS, Cain VA, Waterton JC, Hamar W, Hatsukami TS. Effect of rosuvastatin therapy on carotid plaque morphology and composition in moderately hypercholesterolemic patients: A high-resolution magnetic resonance imaging trial. Am Heart J 2008;155:8.
Underhill HR, Hatsukami TS, Cai J, Yu W, DeMarco JK, Polissar NL, Ota H, Zhao X, Dong L, Oikawa M, Yuan C. A noninvasive imaging approach to assess plaque severity: The carotid atherosclerosis score. Am J Neuroradiol 2010;31:1068–1075.
Wang JN, Bornert P, Zhao HL, Hippe DS, Zhao XH, Balu N, Ferguson MS, Hatsukami TS, Xu JR, Yuan C, Kerwin WS. Simultaneous noncontrast angiography and intraplaque hemorrhage (SNAP) imaging for carotid atherosclerotic disease evaluation. Magn Reson Med 2013;69:337–345.
Wan J, He F, Zhao Y, Zhang H, Zhou X, Wan M. Non-invasive vascular radial/circumferential strain imaging and wall shear rate estimation using video images of diagnostic ultrasound. Ultrasound Med Biol 2014;40:622–636.
Widman E, Caidahl K, Heyde B, D'Hooge J, Larsson M. Ultrasound speckle tracking strain estimation of *in vivo* carotid artery plaque with *in vitro* sonomicrometry validation. Ultrasound Med Biol 2015;41:77–88.
World Health Organization. The atlas of heart disease and stroke. Geneva: Author; 2012.
Yuan C, Mitsumori LM, Beach KW, Maravilla KR. Carotid atherosclerotic plaque: Noninvasive MR characterization and identification of vulnerable lesions. Radiology 2001;221:285–299.
Zhang Q, Li CL, Zhou ML, Liao Y, Huang CC, Shi J, Wang YY, Wang WP. Quantification of carotid plaque elasticity and intraplaque neovascularization using contrast-enhanced ultrasound and image registration-based elastography. Ultrasonics 2015;62:253–262.
Zhao XQ, Phan BAP, Chu BC, Bray F, Moore AB, Polissar NL, Dodge JT, Lee CD, Hatsukami TS, Yuan C. Testing the hypothesis of atherosclerotic plaque lipid depletion during lipid therapy by magnetic resonance imaging: Study design of carotid plaque composition study. Am Heart J 2007;154:239–246.
Zhao XH, Underhill HR, Zhao QA, Cai JM, Li FY, Oikawa M, Dong L, Ota H, Hatsukami TS, Chu BC, Yuan C. Discriminating carotid atherosclerotic lesion severity by luminal stenosis and plaque burden A comparison utilizing high-resolution magnetic resonance imaging at 3.0 tesla. Stroke 2011;42:347–353.
Zhou ZC, Li R, Zhao XH, He L, Wang XL, Wang JN, Balu N, Yuan C. Evaluation of 3 D multi-contrast joint intra- and extracranial vessel wall cardiovascular magnetic resonance. J Cardiovasc Magn Reson 2015;17:11.